Biomaterials Science

ROYAL SOCIETY OF CHEMISTRY

PAPER

View Article Online
View Journal | View Issue

Cite this: *Biomater. Sci.*, 2022, **10**, 6315

Lipoprotein interactions with water-soluble NIR-II emitting aza-BODIPYs boost the fluorescence signal and favor selective tumor targeting†

Ghadir Kalot,[a] Amélie Godard,[b] Benoit Busser,[a,c,d] Mohamed Bendellaa,[a] Fabien Dalonneau,[a] Catherine Paul,[e] Xavier Le Guével,[a] Véronique Josserand,[a,f] Jean-Luc Coll,[a] Franck Denat,[b] Ewen Bodio,[b] Christine Goze,[b] Thomas Gautier[g] and Lucie Sancey *[a]

Following intravenous administration, the interaction of fluorescent exogenous molecules with circulating endogenous transporters can influence their photophysical properties as well as their fate and distribution, and possibly their recognition by different cell types. This type of interaction can be used to optimize the drug delivery but also the imaging properties of a compound of interest. In this study, we investigated the behavior of SWIR-WAZABY-01 fluorophore, a water-soluble aza-BODIPY dye emitting in the NIR-II region, both *in vitro* and *in vivo*. While the fluorescence emission of SWIR-WAZABY-01 was weak in aqueous solutions, it was intensely magnified in plasma (~ ×30). Further analyses using lipoprotein gel electrophoresis and ultracentrifugation revealed interactions between SWIR-WAZABY-01 and plasma lipoproteins *in vitro* and *ex vivo*, in particular with LDL. The tumor uptake mechanism of SWIR-WAZABY-01 was investigated based on the presence of low-density lipoprotein (LDL) receptors and passive tumor uptake. Overall, we found that SWIR-WAZABY-01 interacts with lipoproteins enhancing their NIR-II fluorescence emission, and driving the tumor accumulation with regards to the expression of lipoprotein receptors (LDLR, SR-BI). Moreover, SWIR-WAZABY-01, by exploiting endogenous lipoproteins, arises as a new, potent and relevant tool to efficiently label LDL involved in pathologies.

Received 9th August 2022,
Accepted 18th September 2022

DOI: 10.1039/d2bm01271e

rsc.li/biomaterials-science

1. Introduction

Twenty years ago, fluorescence imaging in the NIR-II window (1000–1700 nm) emerged with the seminal works of H. Dai.[1] Providing less photon scattering and reduced autofluorescence, NIR-II imaging has surpassed imaging in the NIR-I region (700–1000 nm), resulting in images with higher resolution in depth and enhanced signal-to-noise ratio.[2] Pioneering NIR-II fluorophores were inorganic dyes including single-walled carbon nanotubes (SWCNTs),[3] quantum dots,[4] rare-earth doped nanoparticles,[5] and gold nanoclusters.[6,7] Organic NIR-II fluorophores were also developed based on donor–acceptor–donor systems[8] and cyanine dyes.[9] Despite promising tumor imaging capacities in preclinical tumor models, some of these NIR-II fluorophores presented long-term toxicities,[10,11] low quantum yields[4,8] and poor water solubilities that hindered their clinical application.

To address these issues, we developed recently a water-soluble organic fluorophore based on an aza-BODIPY platform[12] with unique fluorescence properties in the NIR-II optical window and showing a favorable tumor uptake capacity even in the absence of any carrier. With no toxicities observed, this aza-BODIPY named SWIR-WAZABY-01 might hold great promise for clinical translation. In the perspective of using SWIR-WAZABY-01 for NIR-II fluorescence-guided surgery, it is important to evaluate its ability to accumulate strongly and specifically in tumors and to explore the mechanism by which SWIR-WAZABY-01 accumulates in different tumor types.

Once introduced into the organism, exogenous molecules may interact with endogenous biomolecules, acquiring a

[a]*Université Grenoble Alpes, Institute for Advanced Biosciences, INSERM U 1209, CNRS UMR 5309, 38000 Grenoble, France.*
E-mail: Lucie.sancey@univ-grenoble-alpes.fr
[b]*Institut de Chimie Moléculaire de l'Université de Bourgogne, Université Bourgogne Franche-Comté, CNRS UMR 6302, Dijon, France*
[c]*Institut Universitaire de France (IUF), France*
[d]*Grenoble Alpes University Hospital (CHUGA), Grenoble, France*
[e]*Laboratoire d'Immunologie et Immunothérapie des Cancers, EPHE, PSL Research University, Université de Bourgogne, Dijon, France*
[f]*OPTIMAL, Small animal Imaging Platform, 38000 Grenoble, France*
[g]*INSERM UMR1231, UFR Sciences de santé, Université Bourgogne Franche-Comté, Dijon, France*

† Electronic supplementary information (ESI) available. See DOI: https://doi.org/10.1039/d2bm01271e

unique biological identity that will influence their biodistribution, pharmacokinetics, and fate *in vivo.*[13] Among the endogenous molecules, interactions with plasma proteins, especially albumin, have been widely studied.[14,15] However, limited studies have addressed the interaction of exogenous molecules with less abundant species such as plasma lipids[16] or lipoproteins.[17] Lipoproteins are natural macromolecular complexes composed of lipids and apolipoproteins.[18] They allow the transport of water-insoluble lipids (cholesterol, triglycerides...) in the blood circulation. Factors such as size, density, type of apolipoproteins and lipid composition define different classes of lipoproteins, the main ones being chylomicrons, very low-density lipoproteins (VLDL), low-density lipoproteins (LDL) and high-density lipoproteins (HDL).[19]

Cancer-related metabolic alterations are associated with higher demand for cholesterol that is required for cell proliferation and formation of new cell membranes.[20] LDL and HDL are a major source of cholesterol for tumor cells, evidenced by the elevated expression of LDL and HDL lipoprotein receptors at their surface: LDL receptor (LDLR)[21,22] and Class B Scavenger receptor BI (SR-BI),[23,24] are present and sometimes overexpressed in multiple cancer types. In this context, LDL and HDL lipoproteins have been proposed as an attractive platform to deliver imaging[25,26] and therapeutic molecules into tumors,[27,28] taking advantage of their biocompatibility, biodegradability, long-circulation time, and selective targeting toward cells overexpressing LDL and HDL lipoprotein receptors. Both isolated lipoproteins (from blood plasma) and synthetic ones have been tested for tumor targeting. Their specific cell targeting capacity has been demonstrated *in vitro*, and *in vivo* in tumor expressing high or low level of lipoproteins receptors.[29] In addition to receptor-mediated uptake *in vivo*, the passive tumor uptake, also called the enhanced permeability and retention (EPR) effect, is widely described in preclinical studies.[30,31]

To evaluate the potential of the SWIR-WAZABY-01 for fluorescence guided surgery of cancer, the dye was administered intravenously to mice-bearing tumors from various origins: glioblastoma (U-87 MG), pancreatic carcinoma (PANC-1), Head and Neck carcinoma (CAL-33), and ovarian adenocarcinoma (SKOV-3 and OVCAR-3). We observed significant differences in SWIR-WAZABY-01 tumor uptake between the different tumor types. We investigated the possible interactions of the fluorophore with plasma components, including the lipoproteins. We observed that lipoproteins in general, and LDL in particular act as endogenous carriers for SWIR-WAZABY-01, and boost the fluorescence emission of the dye. Moreover, the tumor accumulation was related to the expression level of lipoprotein receptors (LDLR, SR-BI).

2. Materials and methods

NIR-II imaging

NIR-II fluorescence imaging was performed using a Princeton camera 640ST (900–1700 nm) coupled to a laser excitation source of λ = 808 nm (100 mW cm^{-2}). We use a short-pass excitation filter at 1000 nm (Thorlabs), and a set of long-pass filters on the emission at 1064 nm (Semrock) and 1250 nm (Thorlabs) were added to the NIR-II camera. A 25 mm lens with 1.4 aperture (Navitar) was used to focus on the mice and drops.

In vivo NIR-II imaging of mice bearing subcutaneous tumors

All the animal experiments were approved by the Animal Ethics Committee of the French Ministry, under the agreement number APAFIS#8782-2017032813328550, and were performed according to the Institutional Animal Care and Use Committee of Grenoble Alpes University. These experiments were carried out within OPTIMAL Grenoble, the Small Animal Imaging Platform of the Institute for Advanced Biosciences.

Female NMRI nude mice (6-week-old) (Janvier Labs, Le Genest-Saint Isle, France) were subcutaneously injected on their right flank with either 5 millions of human glioblastoma astrocytoma U-87 MG cancer cells or 8 millions of human pancreatic carcinoma of ductal cell origin PANC-1 cancer cells, or 5 millions of human tongue squamous cell carcinoma CAL-33 cancer cells, or 10 millions of human ovarian adenocarcinoma SKOV-3 cancer cells, or 8 millions of human ovarian adenocarcinoma OVCAR-3 cancer cells (n = 3 mice/condition). The cell lines were obtained from the European Collection of Authenticated Cell Cultures (ECACC, French authorization CODECOH DC-2020-4226). They were cultured in a 37 °C humidified environment containing 5% CO_2, and in DMEM media supplemented with 10% heat-inactivated fetal bovine serum. For U-87 MG cell cultures 1% non-essential amino acids were added.

Following tumor growth, the mice were intravenously injected in the tail vein with 200 μL of 600 μM SWIR-WAZABY-01 solution diluted in PBS. Whole-body NIR-II fluorescence imaging was performed before and 5, 24 and 48 h after administration. After 48 h, the mice were euthanized and their organs were sampled for *ex vivo* fluorescence imaging. Exposure time was similar for all the conditions. Acquired images were analyzed using Fiji software, and semi-quantitative fluorescence data were obtained by drawing regions of interest (ROI) on the organs.

NIR-II imaging of SWIR-WAZABY-01 solutions in complex environment

150 μM SWIR-WAZABY-01 solution was serially diluted in blood plasma, bovine serum albumin (BSA) 40 g L^{-1}, glucose 5%, sodium chloride (NaCl) 0.9% and phosphate buffered saline (PBS) solution. 10 μL of the diluted samples were dropped on a paraffin paper and imaged by NIR-II camera. Similarly, NIR-II images of SWIR-WAZABY-01 diluted in normal and fat-enriched plasmas were acquired using the long-pass filter at 1250 nm.

Experimental conditions

The following conditions were used for incubation prior to analyses using lipoprotein gel electrophoresis and lipoprotein

ultracentrifugation. 150 μL of each condition were prepared. A 100 μM SWIR-WAZABY-01 solution was selected to obtain a strong fluorescence signal without quenching. LDL, HDL and VLDL, isolated from human and mice blood plasma by density-gradient ultracentrifugation were used at their physiological concentrations indicated by "[ ]p" in Table 1.

Lipoprotein electrophoresis on agarose gel

Lipoprotein gel electrophoresis (BIOTEC-FISCHER Agarose Gel Kit LPE) separates plasma lipoproteins (LDL, VLDL and HDL) according to their electrostatic charges.

Five (5) μL of each experimental condition were loaded onto the agarose gel. Following 30 min of migration, the gel was fixed and dried according to manufacturer's instructions. Fluorescence imaging of the gel was performed to localize the SWIR-WAZABY-01 (ChemiDoc MP imaging system with $\lambda_{Ex.}$ = 835 nm and $\lambda_{Em.}$ = 850 nm), then Sudan Black staining allowed to localize the different lipoproteins. Superimposing the fluorescence and the black/white images allowed the determination of possible SWIR-WAZABY-01-lipoprotein interactions.

Lipoprotein ultracentrifugation

A three-step sequential ultracentrifugation, in TLA100 rotor (Beckman, Palo Alto, CA), was used to fractionate blood plasma into three lipoprotein fractions (VLDL, LDL and HDL) and free proteins according to their densities: VLDL fraction (d < 1.006), LDL fraction (1.006 < d < 1.063), HDL fraction (1.063 < d < 1.21) and protein fraction (d > 1.21). Densities were adjusted by mixing the samples with PBS or KBr solutions ([KBr]) of the appropriate density.

The sequential ultracentrifugation was done as follows:

First run: 50 μL of plasma gently mixed with 150 μL of PBS, in a thick wall polycarbonate tube (230 μL, 7 × 20 mm – 4000 Pk, Beckman Coulter), was subjected to an ultracentrifugation run of 100 000 turns per min for 2 h, leading to the separation of VLDL (supernatant). Second run: the non-separated components of the 1st run (infranatant, 50 μL) were collected, mixed with 50 μL of [KBr] = 1.125 and 100 μL of [KBr] = 1.063, and subjected to a second ultracentrifugation run at 100 000 rpm for 3 h. By the end of the second run, LDL were present in the supernatant and collected. Third run: the non-separated components of the 2nd run (infranatant, 50 μL) were collected, mixed with 50 μL of [KBr] = 1.357 and 100 μL of [KBr] = 1.21, and subjected to a third ultracentrifugation run at 100 000 rpm for 5.5 h. This final step separated the HDL (supernatant) from free proteins (infranatant).

Overall, 50 μL of each experimental condition was subjected to sequential ultracentrifugation, resulting in four fractions (VLDL, LDL, HDL and free proteins). These fractions (50 μL each) were transferred into a black bottom 96-well-plate, and the fluorescence of SWIR-WAZABY-01 was collected at 850 nm following its excitation at 638 nm (TECAN plate reader) and NIR-II imaging system described before (in the form of 10 μL drops).

In vivo experimental conditions for lipoprotein gel electrophoresis and ultracentrifugation

To study the interaction between SWIR-WAZABY-01 and lipoproteins *in vivo*, wild type C57Bl/6J mice (n = 3) and LDLR knockout mice (n = 3) (B6.129S7-Ldlrtm1Her/J, Strain #:002207, The Jackson Laboratory) were intravenously injected in their tail vein with 200 μL of 300 μM SWIR-WAZABY-01 solution diluted in PBS. One mouse of each mice strain served as control (injected with 200 μL PBS only). Thirty minutes following injection, the blood was collected into heparin tubes and centrifuged at 8000 rpm for 8 minutes. The plasma (supernatant) was collected and subjected to Lipoprotein gel electrophoresis and Lipoprotein ultracentrifugation, as described earlier.

Western blot

U-87 MG, PANC-1 and CAL-33 tumor cells cultured in 2D were harvested, washed with PBS, lysed and their protein content was quantified using Micro BCA™ Protein Assay Kit (Thermo Fisher Scientific). Forty micrograms of protein/cell line were loaded into a 12% polyacrylamide gel. Following migration/electrophoresis, the proteins were transferred onto an activated PVDF (polyvinylidene difluoride) membrane (#10600023, Amersham). The membrane was then blocked with 5% milk for 1 h, at RT, and incubated with primary antibodies overnight at 4 °C: anti-LDL receptor antibody (1/1000, Abcam [EP1553Y] (ab52818)), anti-scavenging receptor SR-BI antibody (1/2000, Abcam [EPR20190] (ab217318)), and anti-GAPDH antibody (1/1000, SC-365062, Santa Cruz Biotechnology) serving as loading and transfer control. The membrane was then incubated with the secondary antibodies, anti-mouse/rabbit-horseradish peroxidase HRP (1/3000, #7076S, Cell Signaling Technology) for 1 h, at RT. The proteins (LDLR/SR-B1/GAPDH) were finally revealed using Clarity Western ECL Substrate (Bio-Rad), and western blot imaging was performed using Fusion FX (Vilber). LDLR/SR-BI bands intensities were quantified and

Table 1 Experimental conditions assessed using lipoprotein gel electrophoresis and lipoprotein ultracentrifugation

Experimental condition	Final volume, 150 μL (100 μM SWIR-WAZABY-01)	
PBS + plasma	15 μL PBS	135 μL plasma
SWIR-WAZABY-01 + PBS	15 μL SWIR-WAZABY-01	135 μL PBS
SWIR-WAZABY-01 + plasma	15 μL SWIR-WAZABY-01	135 μL plasma
SWIR-WAZABY-01 + LDLp	15 μL SWIR-WAZABY-01	135 μL [LDL]p = 1.5 g L^{-1}
SWIR-WAZABY-01 + HDLp	15 μL SWIR-WAZABY-01	135 μL [HDL]p = 0.45 g L^{-1}
SWIR-WAZABY-01 + VLDLp	15 μL SWIR-WAZABY-01	135 μL [VLDL]p = 0.5 g L^{-1}

normalized to GAPDH bands in each cell line, using ImageJ software.

Immunohistochemical analyses

Excised tumor tissues (U-87 MG, PANC-1, CAL-33) were frozen in OCT-embedding medium (VWR international, Fontenay-sous-Bois, France), cut into 7 µm thick sections using a cryomicrotome and mounted onto SuperFrost Ultra Plus slides (Thermo Fisher Scientific). The sections were then fixed with 4% formalin, subjected to heat-mediated antigen retrieval, blocked with BLOXALL (SP600, Vector laboratories) and 2.5% horse serum (MP 7401, Vector laboratories), incubated with primary antibodies (anti-LDLR antibody [EP1553Y] (ab52818) or SR-BI antibody [EPR20190] (ab217318)) overnight at 4 °C, incubated with secondary antibody ImmPRESS™ HRP Polymer Anti-Rabbit IgG for 30 min at RT, and revealed using ImmPACT™ NovaRED™ Diluent (SK 4805, Vector laboratories). To localize the nucleus, the slides were counterstained with Hematoxylin. Finally, the slides were dehydrated using ethanol and xylene, mounted with merckoglass and cover slips. The sections were imaged using Zeiss AxioImager M2 microscope.

3. Results

Recently, we developed the first water-soluble aza-BODIPY dye[12] (Fig. 1a) emitting in the NIR-II window (named SWIR-WAZABY-01), with a maximum emission peak at 960 nm and an emission tail reaching 1200 nm (Fig. 1b and c), and

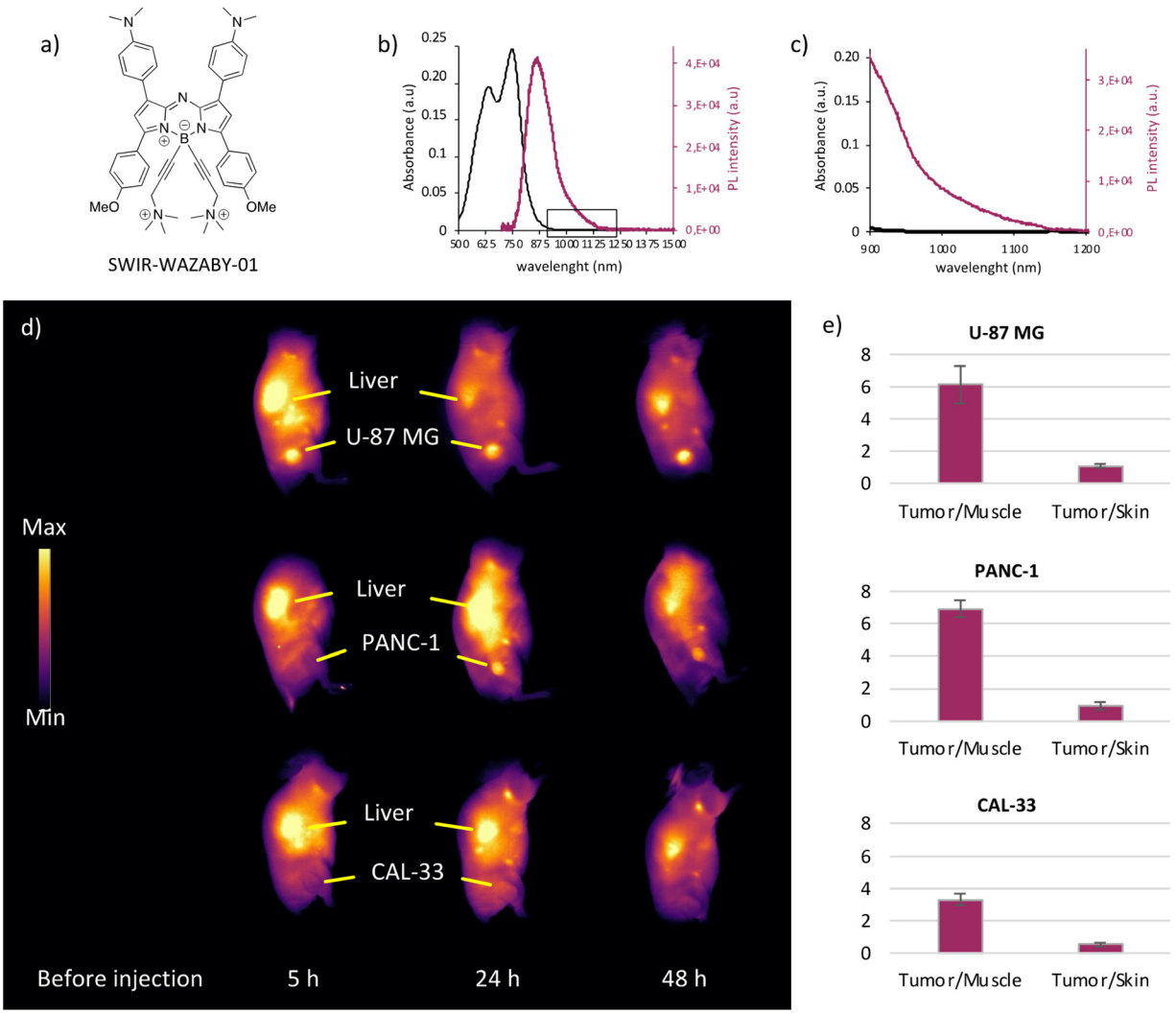

Fig. 1 SWIR-WAZABY-01 properties and tumor-dependent accumulation. (a) Structure of the water-soluble NIR-II emitting SWIR-WAZABY-01. (b) Absorption (black line) and fluorescence emission spectra (purple line) of SWIR-WAZABY-01 in mouse plasma. (c) Expansion of the spectra shown in (b). (d) NIR-II fluorescence imaging of mice bearing subcutaneous U-87 MG, PANC-1, and CAL-33 tumors before and at 5, 24 and 48 h post intravenous administration of SWIR-WAZABY-01 (200 µL at 600 µM). Tumors and livers are indicated by yellow arrows (n = 3 per group). (e) *Ex vivo* tumor/muscle and tumor/skin ratios calculated from excised organs (n = 3 per group). (Adapted with permission from KALOT *et al.*, *Bioconjugate Chem.* 2020, copyright © 2020, American Chemical Society).

evaluated its capability for tumor imaging *in vivo* (Fig. S1†). Without any specific targeting moiety, SWIR-WAZABY-01 clearly accumulated in subcutaneous U-87 MG tumors, with prolonged retention times up to one week, and favorable tumor to healthy tissue ratios (Fig. S1a and b†). It was mainly eliminated by the hepatic route (Fig. S1c†) and no systemic toxicities were observed. Altogether these data presented SWIR-WAZABY-01 as a promising candidate for biomedical applications, in particular for NIR-II fluorescence-guided surgery.[12]

Considering that SWIR-WAZABY-01 has favorable NIR-II fluorescence properties and shows significant uptake in U-87 MG tumors (both subcutaneous[12] and orthotopic tumors, see Fig. S1 and S2† for biodistribution), we investigated the biological behavior of the fluorophore and its tumor accumulation properties in different tumor types. The fluorophore was administered to mice bearing subcutaneous tumors of different origins: U87-MG (human glioblastoma astrocytoma), PANC-1 (human pancreatic carcinoma of ductal cell origin), CAL-33 (human tongue squamous cell carcinoma), SKOV-3 and OVCAR-3 (human ovarian adenocarcinomas) (see ESI for SKOV-3 and OVCAR-3, Fig. S3†). SWIR-WAZABY-01 reached and accumulated in U-87 MG and PANC-1 tumors (Fig. 1d), and the tumors were clearly evidenced at both 24 and 48 h post administration. On the contrary, CAL-33, SKOV-3 and OVCAR-3 tumors were difficult to visualize at the different imaging time points (Fig. 1d, Fig. S3a†). Furthermore, *ex vivo* imaging of U-87 MG and PANC-1 tumors displayed favorable Tumor/Muscle ratios (>6), which were twice higher than those achieved by CAL-33, SKOV-3 and OVCAR-3 tumors (Fig. 1e, Fig. S3b†). This variation in SWIR-WAZABY-01 tumor uptake could be attributed to cell-type dependent passive tumor accumulation through variable enhanced permeability and retention effect (EPR effect) and/or could reveal a specificity in tumor accumulation induced by a selective tumor targeting mechanism.

To evaluate both hypotheses and to understand the mechanism of tumor accumulation, we focused our attention to the plasma distribution of this NIR-II emitting fluorophore, and we investigated whether the fluorophore circulates freely, or linked to proteins, or coupled with other plasma components. To this end, the fluorophore was serial diluted in several media before measuring their NIR-II fluorescence. As indicated in Fig. 2a, c and Fig. S4a, d,† SWIR-WAZABY-01 fluorescence was quenched in PBS, NaCl 0.9% and glucose 5% solutions. When diluted in the presence of 40 g L^{-1} of albumin, the fluorescence was faintly restored, which may indicate a weak association of the probe with the protein. However, when diluted in human plasma, SWIR-WAZABY-01 emitted a strong fluorescence, as indicated by the restauration of the drops' fluorescent signal at a level similar to what is observed in DMSO (Fig. S4a†). Therefore, we postulated that some interactions with plasma components, other than albumin, significantly drive the SWIR-WAZABY-01 distribution and optical properties. The mixing of the SWIR-WAZABY-01 with dyslipemic (fat-rich) human plasma further enhanced its

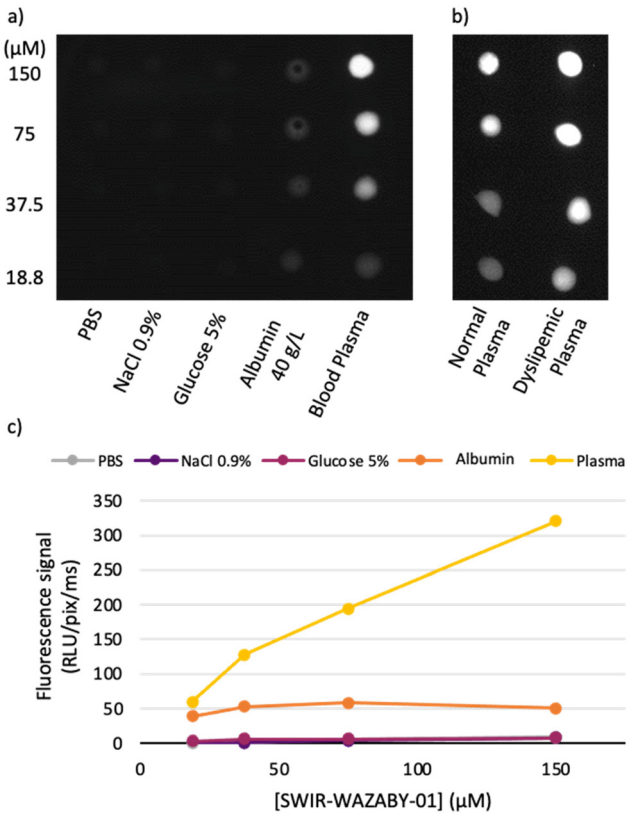

Fig. 2 SWIR-WAZABY-01 medium-dependent fluorescence. (a) NIR-II fluorescence image of SWIR-WAZABY-01 (150 μM) serial dilution in phosphate buffered saline (PBS), sodium chloride (NaCl) 0.9%, glucose 5%, albumin 40 g L^{-1}, and blood plasma. (b) NIR-II fluorescence image of SWIR-WAZABY-01 serial dilution in normal and dyslipemic (fat-rich) human blood plasma. (c) Quantification of the drops' fluorescence from (a).

fluorescence compared to normal plasma (Fig. 2b, Fig. S4b and c†). The strong fluorescence enhancement suggested that plasma lipids or lipoproteins may play a role in the SWIR-WAZABY-01 fluorescence, and may interact directly with the dye.

To explore this hypothesis, SWIR-WAZABY-01 was incubated with human plasma or human lipoproteins, before separating the different components using gel electrophoresis and sequential ultracentrifugation. First, lipoprotein gel electrophoresis allows for the separation of the main human plasma lipoproteins, *i.e.* LDL, VLDL and HDL (Fig. 3a and b), according to their electrostatic charges. In this first experiment, the lipoproteins were revealed on the gel by Sudan black staining and the fluorescence signal was recorded. In absence of fluorophore, no fluorescence signal was evidenced in the plasma (Fig. 3b, lane 1). In absence of plasma, SWIR-WAZABY-01 fluorescence signal migrated in direction of the anode (lane 2) in a faint and diffuse band (red signal). A colocalization between SWIR-WAZABY-01 fluorescence signal and the lipoprotein bands was observed in the mix of SWIR-WAZABY-01 and plasma (lane 3). The main interaction matched with the LDL

a)

Lipo-protein	Size (nm)	Density (g/mL)	Charge (-mV)
VLDL	30 - 80	0.950 - 1.006	6 - 10
LDL	21 - 27	1.019 - 1.063	4 - 6
HDL	7 - 13	1.063 - 1.210	10 - 12

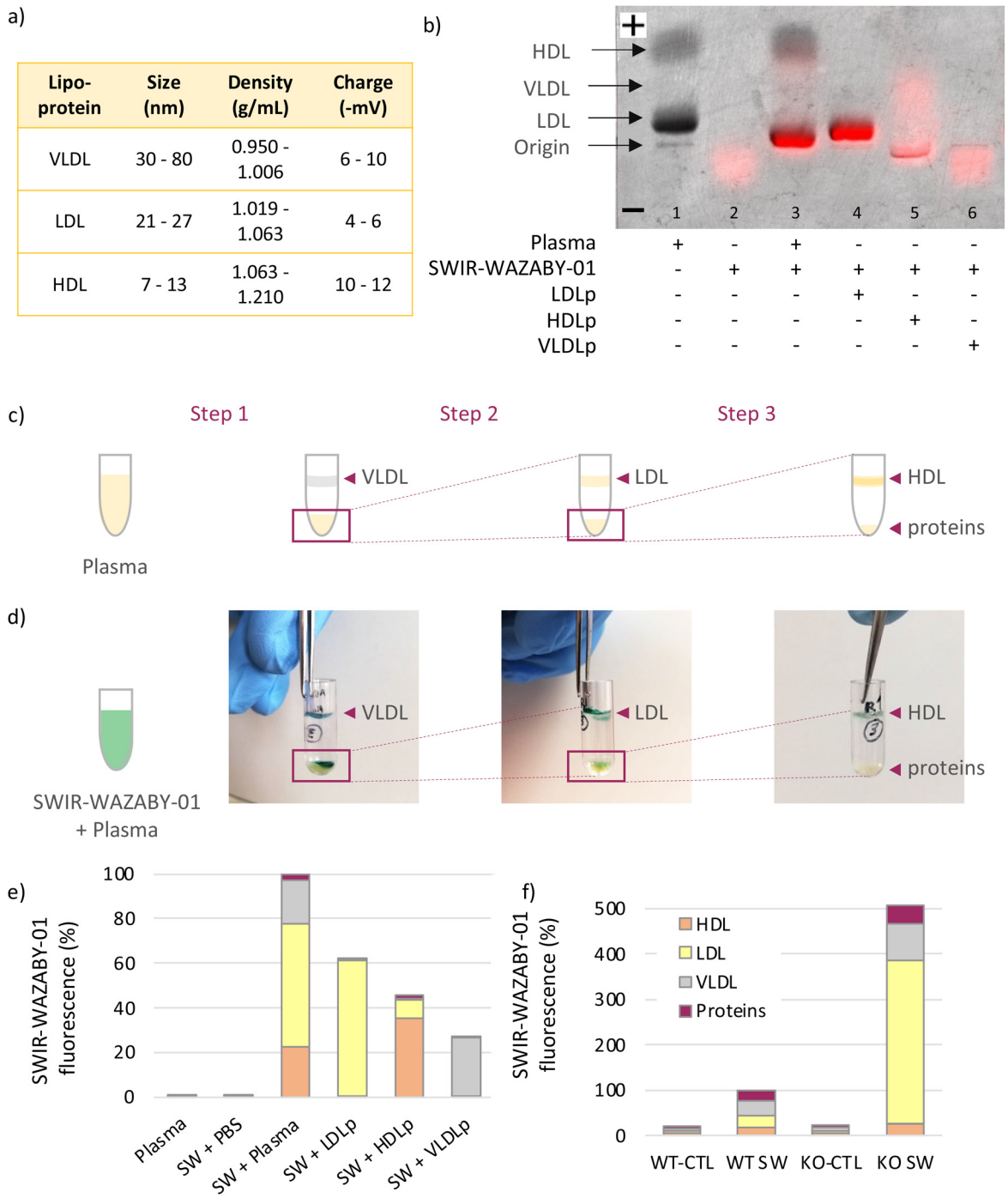

Fig. 3 SWIR-WAZABY-01 interaction with plasma lipoproteins revealed by lipoprotein gel electrophoresis and ultracentrifugation. (a) Table summarizing lipoproteins characteristics.[32,33] (b) Overlay of the SWIR-WAZABY-01 fluorescence image and the black/white image of the lipoprotein electrophoresis gel. SWIR-WAZABY-01 fluorescence is designated by red color while the lipoprotein bands (LDL, VLDL, HDL) are detected in grey, after Sudan Black staining. (c) Illustration of the three-step ultracentrifugation assay of human blood plasma, resulting in the separation of plasma lipoproteins (VLDL, LDL and HDL) and proteins, according to their densities. (d) Pictures illustrating the SWIR-WAZABY-01 (blue-green color) co-localization with plasma lipoproteins (VLDL, LDL, HDL) after each ultracentrifugation step, in the SWIR-WAZABY-01 + plasma condition. (e) Quantification of SWIR-WAZABY-01 (SW) fluorescence in the 4 ultracentrifugation fractions (VLDL, LDL, HDL and free proteins) of each experimental condition (Ex. 808 nm; Em. >1064 nm). (f) Quantification of SWIR-WAZABY-01 fluorescence in the 4 ultracentrifugation fractions (VLDL, LDL, HDL and free proteins) of blood collected from wild type mice (WT) or LDLR KO (KO) mice (n = 3/condition, Ex. 808 nm; Em. >1064 nm), without injection (control conditions, CTL) or 30 min after intravenous administration of SWIR-WAZABY-01 (SW).

band. This strong colocalization pattern was also detected in lane 4 containing the SWIR-WAZABY-01 mixed with a single lipoprotein fraction of LDLp ("p" stands for physiological concentration). On the contrary, weak colocalizations were observed in presence of SWIR-WAZABY-01 mixed with HDLp, or VLDLp (lane 5, and 6 respectively). All together these data demonstrate that the SWIR-WAZABY-01 fluorophore interacts with plasma lipoproteins, mainly with the LDL and to a lesser extent with HDL and VLDL. Interestingly, the interaction of SWIR-WAZABY-01 with lipoproteins consistently led to a reduction of the electronegative charges as illustrated by a shift toward the cathode when compared to plasma incubated in the absence of fluorophore. This is consistent with the migration of the fluorophore alone toward the cathode. The size of the SWIR-WAZABY-01/LDL lipoproteins complex should be comparable with the size of LDL lipoproteins alone, *i.e.*, 21–27 nm, as the aza-BODIPYs are small molecules of about 1 nm in size.

To further confirm the SWIR-WAZABY-01-lipoprotein interactions, lipoproteins were also isolated from human plasma using ultracentrifugation. Following a 3-step sequential ultracentrifugation of plasma, 4 fractions were separated according to their densities, corresponding to VLDL, LDL, HDL and free proteins respectively (Fig. 3c). The SWIR-WAZABY-01 solution, whose color is blue-greenish, allowed the identification of the fluorophore within the fractions before its quantification. A co-localization between the SWIR-WAZABY-01 and the three lipoproteins' fractions (VLDL, LDL, and HDL) was observed after each ultracentrifugation run of the mix SWIR-WAZABY-01 and human plasma solution, while no co-localization was observed with the protein fraction (Fig. 3d). Furthermore, the fluorescence of the 4 fractions (VLDL, LDL, HDL and free proteins) of each experimental condition was quantified (Fig. 3e). The results evidenced that within the mix SWIR-WAZABY-01 and plasma, the LDL fraction contained the major fluorescence signal (~55% of total), followed by VLDL (~25%) and HDL (~20%) fractions, whereas no substantial to weak fluorescence was detected in the free protein fraction. Interestingly, in the mix of SWIR-WAZABY-01 and single fraction of LDLp the major interaction of the dye was evidenced with the LDL, and very weak fluorescence signal was observed within the fraction corresponding to the other lipoproteins VLDL and HDL. Such results were also observed when mixing SWIR-WAZABY-01 and HDLp: a large fraction of the SWIR-WAZABY-01 fluorophore was quantified within the HDL condition (~80%), and the density of the HDL was modified as evidenced by a part of the fluorescence signal detected in the fraction corresponding to the LDL (~20%). The mix SWIR-WAZABY-01 with VLDLp confirmed the moderate interaction of the 2 entities. Very minor fluorescence was detected in the mix of SWIR-WAZABY-01 and PBS, or within the free protein fractions. Altogether, these results supported the hypothesis that the SWIR-WAZABY-01 interacts with plasma lipoproteins, predominantly with the LDL. LDL may therefore play a major role in SWIR-WAZABY-01 transport *in vivo*.

Plasma lipoprotein profile differs between human and mice. Indeed, while LDL are the major lipoproteins in humans (about 60% of cholesterol transport), they are present at low levels in mouse plasma where HDL are the main cholesterol carriers (about 80%).[34] To study the possible interactions of SWIR-WAZABY-01 with mouse lipoproteins and LDL in particular, the fluorophore was injected intravenously to mice, and their blood was sampled after 30 min. Both wild type (WT) and LDL-receptor (LDLR) knockout (KO) mice were used, as LDLR KO mice possess a high level of circulating lipoproteins, especially LDL.[35] Without fluorophore, mouse plasma displayed very low autofluorescence (Fig. 3f, Fig. S5†). After intravenous administration of SWIR-WAZABY-01 in WT mice, the fluorescence was observed in the different lipoprotein fractions. In LDLR KO animals, a strong increase of the fluorescence signal was observed as compared to WT mice (~500%), with a major increase of the LDL fraction *versus* WT animals (×14) reaching almost 70% of the total plasma fluorescence. Similarly to the studies in human plasma, SWIR-WAZABY-01 might interact with lipoproteins in mice, and LDL in particular.

Bearing in mind that *in vivo* SWIR-WAZABY-01 could be distributed in the blood stream *via* lipoproteins, and that several tumors overexpress lipoprotein receptors, we evaluated the influence of tumor lipoprotein receptors expression on SWIR-WAZABY-01 accumulation in tumors. The expression of LDLR and SR-B1 (*i.e.* the main receptors for LDL and HDL, respectively) was evaluated on tumor cell extracts (Fig. 4a and b, Fig. S6†) and on excised tumor sections (Fig. 4c). The western blot analysis indicated a strong expression of the LDLR in the U-87 MG cell line while its expression was very faint or absent in PANC-1, CAL-33, SKOV-3 and OVCAR-3 (see also Fig. S6†). SR-B1 was overexpressed in PANC-1, and weakly expressed or not detected in U-87 MG, CAL-33, SKOV-3 and OVCAR-3. These results were confirmed by immunohistology investigations on different tumor sections: as compared to normal tissue, U-87 MG homogenously overexpressed the LDLR, PANC-1 overexpressed SR-B1, while both receptors were not or poorly expressed in the other cell lines. Thus, the *in vivo* SWIR-WAZABY-01 tumor accumulation was strongly correlated with tumor lipoprotein receptors expression patterns (Fig. 1 and Fig. S3†).

4. Discussion

The development of NIR-II emitting fluorophores for image-guided surgery,[36] aiming at discovering molecules with performant optical properties (brightness, photostability), water-solubility, favorable biological behavior in terms of enhanced pharmacokinetics, selective uptake and long-term retention in the tumor area, is a real challenge. The optimal fluorescence of a compound in physiological media is partially related to its optimal dispersion, to avoid any quenching of the compound. In parallel, the pharmacokinetic properties are partly driven by interactions of the molecule of interest with plasma components. Albumin is the most abundant protein in plasma, and a remarkable carrier for many dyes,[37] or drugs.[38,39] As any other molecule administered in the bloodstream, fluorophores

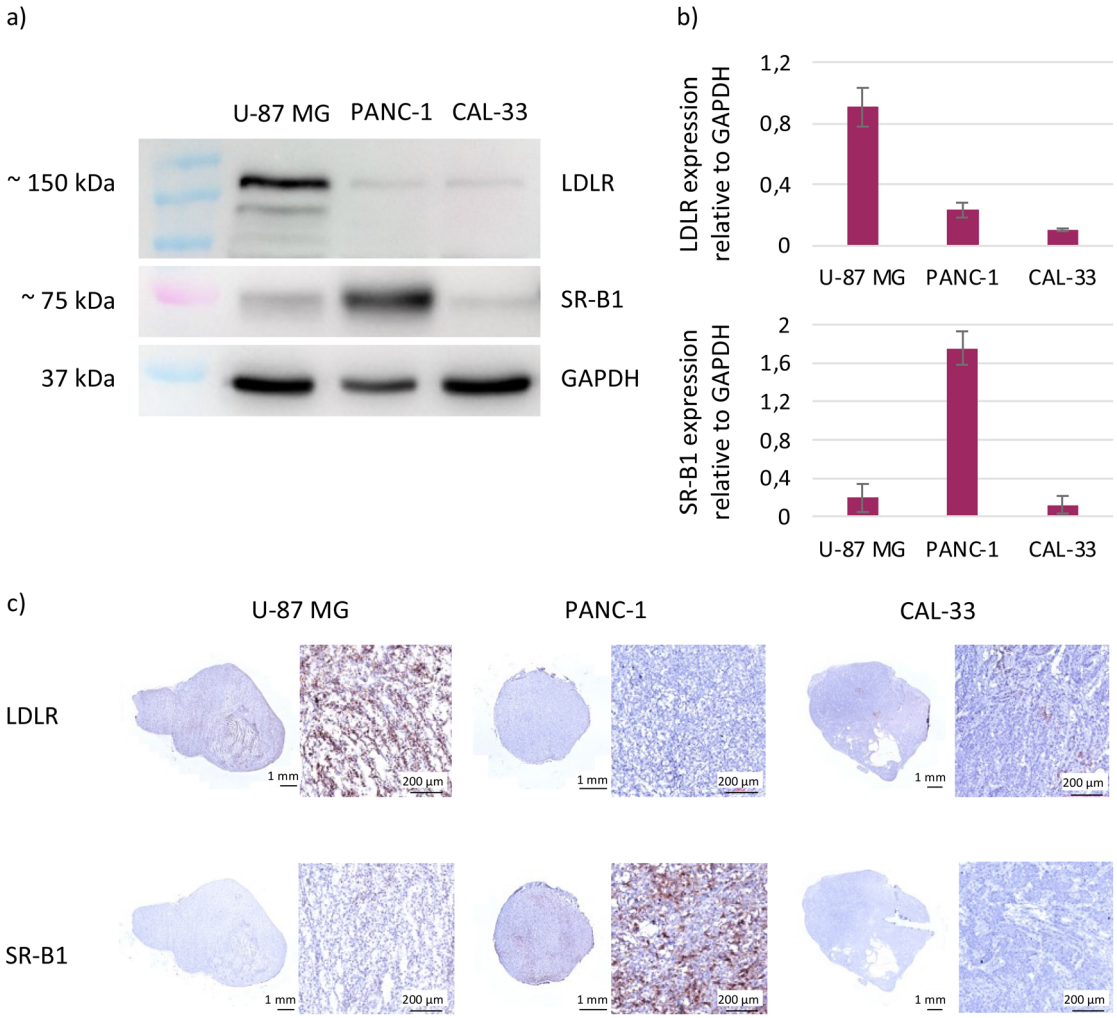

Fig. 4 Lipoprotein receptors expression profile in tumor cells (a) and resected tumors (c). (a) Lipoprotein receptors (LDLR, SR-BI) expression in U-87 MG, PANC-1 and CAL-33 cells, assessed by western blot of whole protein extracts. GAPDH served as a loading control. (b) Quantification of LDLR and SR-BI expression relative to GAPDH obtained from data in (a). (c) Lipoprotein receptors (LDLR, SR-BI) expression in U-87 MG, PANC-1 and CAL-33 excised tumors, detected by immunohistochemical staining.

may also interact with other plasma components. Previously reported studies investigated interactions of some BODIPYs with serum albumin[40] and other blood plasma proteins.[41]

Here, we investigated the possible interaction of the water-soluble NIR-II emitting aza-BODIPY derivative SWIR-WAZABY-01 with albumin and lipoproteins, and evidenced that SWIR-WAZABY-01 fluorophore mainly interacts with LDL lipoproteins, and to lesser extent with HDL and VLDL lipoproteins, in human plasma *ex vivo* (Fig. 3b and e). This finding could be explained by the composition of the human lipoprotein system, with the LDL being the most abundant lipoprotein and with the highest amount of cholesterol.[18]

Despite the functionalization of SWIR-WAZABY-01 on the boron atom that makes the molecule water-soluble,[42] SWIR-WAZABY-01 possesses a large aromatic structure that may facilitate its interactions with lipophilic structures similar to those present in lipoproteins.[43] Similar studies have reported the interaction of the fluorescent indocyanine green (ICG) with the hydrophobic pocket of the albumin.[44] In our case and as expected, the fluorescence emission of the compound is highly dependent of the nature of the solvent. SWIR-WAZABY-01 is strongly fluorescent in DMSO due to its donor–acceptor–donor' properties. In water or PBS, the fluorescence signal was totally quenched, which is common for highly polarized BODIPYs at the exited state, especially structures bearing dimethyl-aniline moieties (in absence of *N*,*N*-dimethylamino groups, the compounds are fluorescent in PBS). Interestingly, the SWIR-WAZABY-01 fluorescence was increased by 150% similar to DMSO, when the SWIR-WAZABY-01 was in presence of blood plasma (Fig. 3b, and Fig. S4†). Moreover, in LDL-enriched plasma, this increase in the fluorescence signal was even higher (≈ ×2 in our conditions, Fig. S4†). Such an increase of the fluorescence has been reported for other fluorophore/lipid complexes, as ICG incorporated into liposomes.[45] The interaction or incorporation of the SWIR-WAZABY-01 within LDL is not clear; however, SWIR-WAZABY-01 may either

insert in-depth or at least is partially protected from water, as water quenches its fluorescence. We can postulate that the association of SWIR-WAZABY-01 with lipoproteins could also help to isolate the fluorophore and/or minimize its vibration or deactivation pathways *via* interaction of the aza-BODIPY with physiological components, participating to the increase of fluorescence.[44]

The interaction of SWIR-WAZABY-01 with the lipoproteins slightly modified both the global charge and density of these lipidic entities. As the fluorophore is positively charged in solution, it increased the positive charge of the lipoproteins, as observed by the migration shift of lipoprotein bands towards the negative end of the membrane when mixed with the aza-BODIPY (Fig. 3b). Similarly, the overall density of the lipidic vectors was decreased in presence of the dye (Fig. 3e). These modifications constitute a further proof of the tight interaction between the probe and the lipoproteins. Additional experiments will be necessary to reveal the exact structure of this interaction.

Since the LDL endocytic pathway and the HDL cholesterol delivery are highly active in malignant cancer cells, the use of LDL and HDL as endogenous drug carriers to target cancer cells has been proposed. Such vectorization has been reported for the delivery of siRNA,[46] genes,[47] chemotherapies,[28,48] anti-cancer drugs,[49] and fluorescent probes.[25,26] However, the complexity of LDL and HDL isolation, storage and drug incorporation strategies, hindered its industrial development. Similarly, the development of synthetic LDL and HDL-like particles is highly complicated. In the present case, the interaction between SWIR-WAZABY-01 and endogenous LDL and HDL occurs spontaneously after SWIR-WAZABY-01 intravenous administration. Therefore, lipoproteins act as natural carriers vectorizing SWIR-WAZABY-01. Similar spontaneous *in vivo* loading of squalenoylated anti-cancer drugs into lipoproteins and cancer targeting have been reported.[50,51]

The tumor accumulation of SWIR-WAZABY-01 could help to specifically identify and delineate tumor lesions characterized with high expression of the LDLR.[25,45] However, this NIR-II emitting fluorophore could also be modified for chemical ligation to a biological ligand (*i.e.* small molecule or antibody) for tumor-related biomarker targeting in fluorescence-guided surgery of cancer.

5. Conclusion

In conclusion, we demonstrated the preferential interaction of the NIR-II emitting SWIR-WAZABY-01 with LDL (~60% of total lipoproteins) which drives its circulation in the bloodstream, strongly increases its fluorescence emission, and favors its uptake in tumor expressing the LDLR. Such natural carrier will be of particular interest for designing the next generation of fluorophore, and for future fluorescence-guided surgery investigations. In addition, such association with LDL in blood circulation could be used to study the LDL accumulation in specific pathologies as atherosclerosis disorders.

Contributions

Conceptualization: G. K., E. B., C. G., T. G., L. S. – investigation: G. K., A. G., M. B., F. D., C. P., E. B., C. G., T. G., L. S. – validation: B. B, X. L. G, V. J., J.-L. C., F. D., E. B., C. G., T. G., L. S. – writing & original draft: G. K., L. S. – review & editing: all authors.

Conflicts of interest

G. K., A. G., B. B, X. L. G, V. J., J.-L. C., F. D., E. B., C. G., L. S. have a patent to declare, related to the fluorescent aza-BODIPY (EP19315089.3/WO2021/023731). The other authors have declared that no competing interest exists.

Acknowledgements

The authors would like to thank Dr Olivier Lamotte (Agroécologie – AgroSup, CNRS, INRAE, University of Burgundy, Dijon) for using the TECAN plate reader, and the research engineer Maxime Henry for technical help in orthotopic glioblastoma tumor implantation.

The research in this paper is funded by FRM ECO201806006861, GDR CNRS AIM mobility grant, Oncostarter project of the cancérôpole CLARA (Agnostic project), France Life Imaging (Thera-BODIPY), GEFLUC Grenoble Dauphiné Savoie, the French National Research Agency (JCJC ANR-18-CE18-0012 and ANR-11-LABX-0021-01-LipSTIC LabEx, Ligue Contre le Cancer AURA).

References

1 K. Welsher, Z. Liu, S. P. Sherlock, J. T. Robinson, Z. Chen, D. Daranciang and H. Dai, *Nat. Nanotechnol.*, 2009, **4**, 773–780.
2 G. Hong, A. L. Antaris and H. Dai, *Nat. Biomed. Eng.*, 2017, **1**, 0010.
3 D. Ghosh, A. F. Bagley, Y. J. Na, M. J. Birrer, S. N. Bhatia and A. M. Belcher, *Proc. Natl. Acad. Sci. U. S. A.*, 2014, **111**, 13948–13953.
4 G. Hong, J. T. Robinson, Y. Zhang, S. Diao, A. L. Antaris, Q. Wang and H. Dai, *Angew. Chem., Int. Ed. Engl.*, 2012, **51**, 9818–9821.
5 D. J. Naczynski, M. C. Tan, M. Zevon, B. Wall, J. Kohl, A. Kulesa, S. Chen, C. M. Roth, R. E. Riman and P. V. Moghe, *Nat. Commun.*, 2013, **4**, 2199.
6 M. Broekgaarden, A. L. Bulin, E. Porret, B. Musnier, B. Chovelon, C. Ravelet, L. Sancey, H. Elleaume, P. Hainaut, J. L. Coll and X. Le Guevel, *Nanoscale*, 2020, **12**, 6959–6963.
7 X. Le Guevel, K. D. Wegner, C. Wurth, V. A. Baulin, B. Musnier, V. Josserand, U. Resch-Genger and J. L. Coll, *Chem. Commun.*, 2022, **58**, 2967–2970.
8 A. L. Antaris, H. Chen, K. Cheng, Y. Sun, G. Hong, C. Qu, S. Diao, Z. Deng, X. Hu, B. Zhang, X. Zhang, O. K. Yaghi,

Z. R. Alamparambil, X. Hong, Z. Cheng and H. Dai, *Nat. Mater.*, 2016, **15**, 235–242.
9 X. Meng, J. Zhang, Z. Sun, L. Zhou, G. Deng, S. Li, W. Li, P. Gong and L. Cai, *Theranostics*, 2018, **8**, 6025–6034.
10 Z. Liu, C. Davis, W. Cai, L. He, X. Chen and H. Dai, *Proc. Natl. Acad. Sci. U. S. A.*, 2008, **105**, 1410–1415.
11 Y. Zhang, Y. Zhang, G. Hong, W. He, K. Zhou, K. Yang, F. Li, G. Chen, Z. Liu, H. Dai and Q. Wang, *Biomaterials*, 2013, **34**, 3639–3646.
12 A. Godard, G. Kalot, J. Pliquett, B. Busser, X. Le Guével, K. D. Wegner, U. Resch-Genger, Y. Rousselin, J. L. Coll, F. Denat, E. Bodio, C. Goze and L. Sancey, *Bioconjugate Chem.*, 2020, **31**, 1088–1092.
13 M. P. Monopoli, C. Aberg, A. Salvati and K. A. Dawson, *Nat. Nanotechnol.*, 2012, **7**, 779–786.
14 A. Tiwari, P. Bhatia and J. K. Randhawa, *Dalton Trans.*, 2020, **49**, 12380–12389.
15 Q. Wang, W. Q. Chen, X. Y. Liu, Y. Liu and F. L. Jiang, *ACS Omega*, 2021, **6**, 5569–5581.
16 A. A. Kapralov, W. H. Feng, A. A. Amoscato, N. Yanamala, K. Balasubramanian, D. E. Winnica, E. R. Kisin, G. P. Kotchey, P. Gou, L. J. Sparvero, P. Ray, R. K. Mallampalli, J. Klein-Seetharaman, B. Fadeel, A. Star, A. A. Shvedova and V. E. Kagan, *ACS Nano*, 2012, **6**, 4147–4156.
17 E. Hellstrand, I. Lynch, A. Andersson, T. Drakenberg, B. Dahlbäck, K. A. Dawson, S. Linse and T. Cedervall, *FEBS J.*, 2009, **276**, 3372–3381.
18 K. R. Feingold, in *Endotext*, ed. K. R. Feingold, B. Anawalt, A. Boyce, G. Chrousos, W. W. de Herder, K. Dhatariya, K. Dungan, A. Grossman, J. M. Hershman, J. Hofland, S. Kalra, G. Kaltsas, C. Koch, P. Kopp, M. Korbonits, C. S. Kovacs, W. Kuohung, B. Laferrère, E. A. McGee, R. McLachlan, J. E. Morley, M. New, J. Purnell, R. Sahay, F. Singer, C. A. Stratakis, D. L. Trence and D. P. Wilson, MDText.com, Inc. Copyright © 2000–2021, MDText.com, Inc., South Dartmouth (MA). South Dartmouth (MA), 2000.
19 S. Busatto, S. A. Walker, W. Grayson, A. Pham, M. Tian, N. Nesto, J. Barklund and J. Wolfram, *Adv. Drug Delivery Rev.*, 2020, **159**, 377–390.
20 Y. K. Ho, R. G. Smith, M. S. Brown and J. L. Goldstein, *Blood*, 1978, **52**, 1099–1114.
21 M. J. Rudling, L. Ståhle, C. O. Peterson and L. Skoog, *Br. Med. J.*, 1986, **292**, 580–582.
22 A. J. Versluis, P. J. van Geel, H. Oppelaar, T. J. van Berkel and M. K. Bijsterbosch, *Br. J. Cancer*, 1996, **74**, 525–532.
23 J. L. Gutierrez-Pajares, C. Ben Hassen, S. Chevalier and P. G. Frank, *Front. Pharmacol.*, 2016, **7**, 338.
24 B. Yuan, C. Wu, X. Wang, D. Wang, H. Liu, L. Guo, X. A. Li, J. Han and H. Feng, *Tumor Biol.*, 2016, **37**, 3581–3588.
25 H. Li, Z. Zhang, D. Blessington, D. S. Nelson, R. Zhou, S. Lund-Katz, B. Chance, J. D. Glickson and G. Zheng, *Acad. Radiol.*, 2004, **11**, 669–677.
26 W. Cao, K. K. Ng, I. Corbin, Z. Zhang, L. Ding, J. Chen and G. Zheng, *Bioconjugate Chem.*, 2009, **20**, 2023–2031.
27 D. Gal, M. Ohashi, P. C. MacDonald, H. J. Buchsbaum and E. R. Simpson, *Am. J. Obstet. Gynecol.*, 1981, **139**, 877–885.
28 L. K. Mooberry, M. Nair, S. Paranjape, W. J. McConathy and A. G. Lacko, *J. Drug Targeting*, 2010, **18**, 53–58.
29 M. Mahmoudian, S. Salatin and A. Y. Khosroushahi, *Cancer Chemother. Pharmacol.*, 2018, **82**, 371–382.
30 A. Karageorgis, S. Dufort, L. Sancey, M. Henry, S. Hirsjarvi, C. Passirani, J. P. Benoit, J. Gravier, I. Texier, O. Montigon, M. Benmerad, V. Siroux, E. L. Barbier and J. L. Coll, *Sci. Rep.*, 2016, **6**, 21417.
31 Y. Shi, R. van der Meel, X. Chen and T. Lammers, *Theranostics*, 2020, **10**, 7921–7924.
32 D. L. Sparks and M. C. Phillips, *J. Lipid Res.*, 1992, **33**, 123–130.
33 M. K. Wojczynski, S. P. Glasser, A. Oberman, E. K. Kabagambe, P. N. Hopkins, M. Y. Tsai, R. J. Straka, J. M. Ordovas and D. K. Arnett, *Lipids Health Dis.*, 2011, **10**, 181.
34 Z. Kaabia, J. Poirier, M. Moughaizel, A. Aguesse, S. Billon-Crossouard, F. Fall, M. Durand, E. Dagher, M. Krempf and M. Croyal, *Sci. Rep.*, 2018, **8**, 15893.
35 G. S. Getz and C. A. Reardon, *Arterioscler., Thromb., Vasc. Biol.*, 2016, **36**, 1734–1741.
36 Y. Xu, C. Li, X. Ma, W. Tuo, L. Tu, X. Li, Y. Sun, P. J. Stang and Y. Sun, *Proc. Natl. Acad. Sci. U. S. A.*, 2022, **119**, e2209904119.
37 R. Tian, Q. Zeng, S. Zhu, J. Lau, S. Chandra, R. Ertsey, K. S. Hettie, T. Teraphongphom, Z. Hu, G. Niu, D. O. Kiesewetter, H. Sun, X. Zhang, A. L. Antaris, B. R. Brooks and X. Chen, *Sci. Adv.*, 2019, **5**, eaaw0672.
38 G. Hartung, G. Stehle, H. Sinn, A. Wunder, H. H. Schrenk, S. Heeger, M. Kränzle, L. Edler, E. Frei, H. H. Fiebig, D. L. Heene, W. Maier-Borst and W. Queisser, *Clin. Cancer Res.*, 1999, **5**, 753–759.
39 P. Schmid, S. Adams, H. S. Rugo, A. Schneeweiss, C. H. Barrios, H. Iwata, V. Diéras, R. Hegg, S. A. Im, G. Shaw Wright, V. Henschel, L. Molinero, S. Y. Chui, R. Funke, A. Husain, E. P. Winer, S. Loi and L. A. Emens, *N. Engl. J. Med.*, 2018, **379**, 2108–2121.
40 A. V. Solomonov, E. V. Rumyantsev, B. A. Kochergin and E. V. Antina, *Biophysics*, 2014, **59**, 35–42.
41 Y. S. Marfin, E. L. Aleksakhina, D. A. Merkushev, E. V. Rumyantsev and I. K. Tomilova, *J. Fluoresc.*, 2016, **26**, 255–261.
42 J. Pliquett, A. Dubois, C. Racoeur, N. Mabrouk, S. Amor, R. Lescure, A. Bettaïeb, B. Collin, C. Bernhard, F. Denat, P. S. Bellaye, C. Paul, E. Bodio and C. Goze, *Bioconjugate Chem.*, 2019, **30**, 1061–1066.
43 R. J. Deckelbaum, G. G. Shipley and D. M. Small, *J. Biol. Chem.*, 1977, **252**, 744–754.
44 V. A. Kuzmin, T. D. Nekipelova, T. A. Podrugina, G. V. Golovina, A. A. Kostyukov, V. V. Temnov, I. A. Doroshenko, E. V. Radchenko, V. A. Palyulin and N. S. Zefirov, *Photochem. Photobiol. Sci.*, 2016, **15**, 1377–1384.
45 J. C. Kraft and R. J. Ho, *Biochemistry*, 2014, **53**, 1275–1283.

46 S. I. Kim, D. Shin, T. H. Choi, J. C. Lee, G. J. Cheon, K. Y. Kim, M. Park and M. Kim, *Mol. Ther.*, 2007, **15**, 1145–1152.
47 J. Varshosaz, H. Vakilzadeh and E. Ghassami, *Curr. Pharm. Des.*, 2016, **22**, 3466–3485.
48 M. Masquelier, S. Vitols, M. Pålsson, U. Mårs, B. S. Larsson and C. O. Peterson, *J. Drug Targeting*, 2000, **8**, 155–164.
49 M. Nikanjam, E. A. Blakely, K. A. Bjornstad, X. Shu, T. F. Budinger and T. M. Forte, *Int. J. Pharm.*, 2007, **328**, 86–94.
50 D. Sobot, S. Mura, S. O. Yesylevskyy, L. Dalbin, F. Cayre, G. Bort, J. Mougin, D. Desmaële, S. Lepetre-Mouelhi, G. Pieters, B. Andreiuk, A. S. Klymchenko, J. L. Paul, C. Ramseyer and P. Couvreur, *Nat. Commun.*, 2017, **8**, 15678.
51 D. Sobot, S. Mura, M. Rouquette, B. Vukosavljevic, F. Cayre, E. Buchy, G. Pieters, S. Garcia-Argote, M. Windbergs, D. Desmaële and P. Couvreur, *Mol. Ther.*, 2017, **25**, 1596–1605.